We are IntechOpen, the world's leading publisher of Open Access books Built by scientists, for scientists

6,900
Open access books available

185,000
International authors and editors

200M
Downloads

Our authors are among the

154
Countries delivered to

TOP 1%
most cited scientists

12.2%
Contributors from top 500 universities

CLARIVATE ANALYTICS
BOOK CITATION INDEX
INDEXED

WEB OF SCIENCE™

Selection of our books indexed in the Book Citation Index
in Web of Science™ Core Collection (BKCI)

Interested in publishing with us?
Contact book.department@intechopen.com

Probing the Thermodynamics of Photosystem I by Spectroscopic and Mutagenic Methods

Xuejing Hou and Harvey J.M. Hou

Additional information is available at the end of the chapter

1. Introduction

Thermodynamics of a chemical reaction is a fundamental and vital issue for complete understanding of the reaction at the molecular level and involves the elucidation of the energy level of reactant and products, direction of reaction, and driving force or spontaneity of the reaction (Tadashi, 2011). Most the chemical reactions are enthalpy driven and are determined by chemical bonding energy of the reactants and products. However, some of the chemical reaction or process is entropy driven and are largely due the probability or disorder of the system during the reaction. Protein denaturation and dissolution of potassium iodide in water are such examples. In chemistry and biology, especially electron transfer reaction, the entropy changes are often assumes small and negligible. The understanding of thermodynamics of electron transfer reactions is relatively limited (Mauzerall, 2006).

To study the thermodynamics of reaction in chemistry and biology, photosynthetic reaction is an excellent model system. The photosynthesis involves multiple electron transfer reaction driven by sunlight under room temperature and neutral pH (Blankenship, 2002; Diner and Rappaport, 2002; Golbeck, 2006). The understanding of light-induced electron transfer reaction in photosynthesis will provide fundamental knowledge of chemical reactions and guide the design and fabrication in artificial photosynthetic system in address the global energy and environmental crisis in the 21st century (Lewis and Nocera, 2006). In particular the solar energy storage of solar energy using water splitting reaction mimicking photosynthesis might solved energy and pure water problems at the same time (Kanan and Nocera, 2008; Cook et al., 2010; Hou, 2010, 2011). The electron transfer reactions in photosynthesis involves four major chlorophyll binding protein complexes: Photosystem II, cytochrome b_6f, photosystem I, and ATP synthase (Figure 1). Photosystem I and photosystem II are belong to two types of different reaction centers in nature, respectively. Type I reaction centers incorporate a phylloquinone or menaquinone as secondary electron

acceptor, A_1, and three tertiary iron-sulfur cluster electron acceptors, F_A, F_B, and F_X. Type II centers use two quinone acceptors: Q_A undergoes one-electron reduction, and Q_B undergoes a two-electron reduction with concomitant protonation.
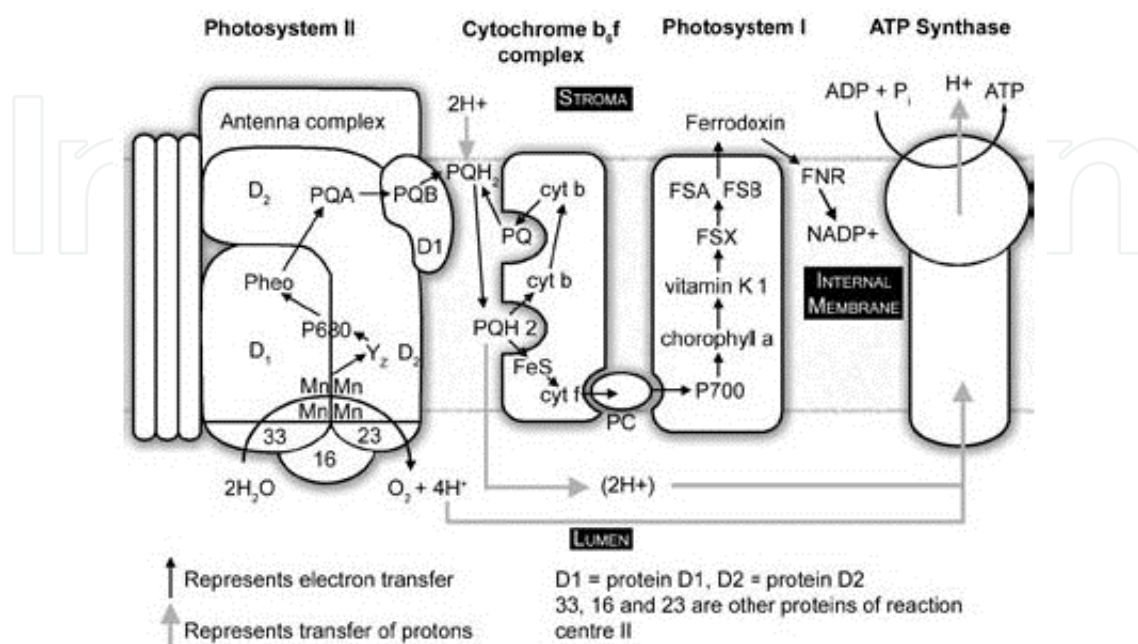

Figure 1. Four protein complexes, including photosystem II, cytochrome b₆f, photosystem I, and ATP synthase, are responsible for the electron transfer reactions in photosynthesis. (from http://www.answersingenesis.org/articles/tj/v17/n3/photosynthesis).

Photosystem I is a pigment-protein complex consisting of more than 11 polypeptides embedded in the photosynthetic membrane and catalyzes light-induced electron transfer from reduced plastocyanin (or cytochrome c_6) to oxidized ferredoxin (or flavodoxin). The electron transfer pathway and the electron transfer cofactors in photosystem I is shown as a black arrows in Figure 1. The primary electron donor is P_{700}, a pair of chlorophyll a molecules. After absorbing light photon energy, P_{700} becomes excited species P_{700}^* and delivers one electron to the primary electron acceptor A_0, a chlorophyll a molecule. The reduced A_0 anion donates its electron to the secondary acceptor A_1, a phylloquione or vitamin K_1 molecule. The reduced A^1 anion transfer the electron to F_X, F_A, F_B, and finally to ferrodoxin for producing $NADPH^+$.

The three-dimensional structure of cyanobacterial PS I at 2.5 A resolution has been obtained and revealed much of the detailed orientation and binding site of electron transfer cofactors. These structural details offer a solid basis for structure and function studies at an atomic level (Figure 2). The almost complete symmetric arrangement of cofactors in PS I suggested the electron transfer might involve two electron transfer branches (A side and B side). This is different from the electron transfer mechanism in type II centers. For example, in bacterial and PS II, only one electron transfer branch (L side or D1 side) is active. The M-side (or D2 side) electron transfer is inactive and may provide protective role in the reaction center in regulating excess light energy.
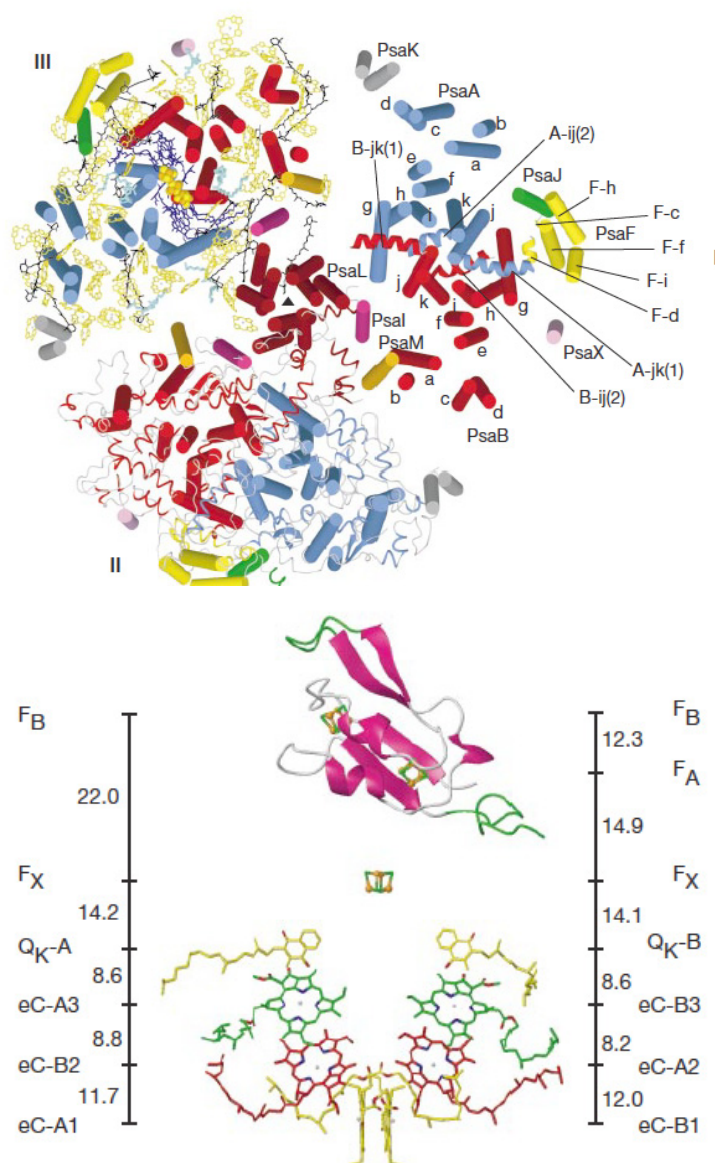
Figure 2. X-ray crystallographic structure (upper panel) and the arrangment of the cofactors (lower pahnel) in photosystem I from cyanobacterium *Synechococcus* elongatus (Jordan et al., 2001) (Reproduced with permission from Nature publishing Group).

2. Quinones in photosystem I

A quinone molecule is a perfect electron transfer cofactor due to its reversible electrochemical redox properties and plays a key role in photosynthetic electron transfer process. For example, both type I and type II reaction centers contain a quinone that operates as an intermediate electron acceptor and as a one-electron carrier. However, the local protein environment and chemical properties of the quinone in these two types of reaction centers must be different. EPR measurements revealed that there are striking difference in the binding and function of phylloquinone (A_1) in PS I and ubiquione (Q_A) in the bacterial center of R. sphaeroides (Kamlowski et al., 1998). As a type I center, PS I

contain a bound menaquinone, usually phylloquinone (A_1, vitamin K1, 2-methyl-3-phytyl-1,4-naphthoquinone). In contrast, PS II uses the plasoquinone (A_P). The chemical structures of A_1 and A_P are shown in Figure 3.

To investigate the function of ubiquinone in bacterial photosynthesis, the native quinone can be removed by organic solvent extraction and replaced with 22 other quinones. The rate of electron transfer in these reconstituted reaction center, Gibbs free energy, enthalpy changes, and apparent entropy changes were determined by EPR, transient time-resolved absorption spectroscopy, theoretical calculation and modeling, and photoacoustic spectroscopy (Gunner and Dutton, 1989; Edens et al., 2000). The molecular volume changes of charge separation due to electrostriction correlates with the size of quinones as expected (Edens et al., 2000). However, the methodology of replacement of quinone is not successful in PS I.
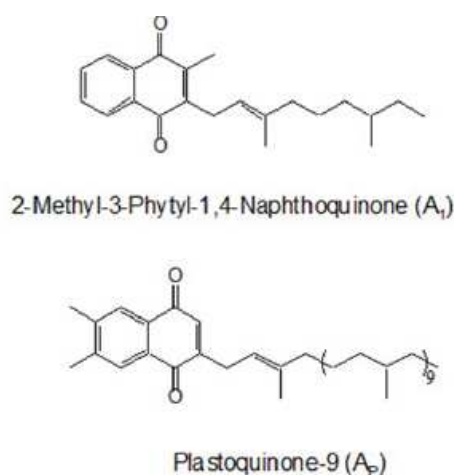

2-Methyl-3-Phytyl-1,4-Naphthoquinone (A_1)

Plastoquinone-9 (A_P)

Figure 3. Chemical structures of quinones in photosynthesis. A_1 is native quinone in photosystem I, and A_P is a plastoquinone in photosystem II.

A biological method to replace phylloquinone was devised by Chitnis and Golbeck (Johnson et al., 2000; Semenov et al., 2000). The strategy to disallow A_1 function is to inactivate genes that code for enzymes involved in the biosynthetic pathway of phylloquinone. The synthesis of the phylloquione in *Synechocystis* sp. PCC 6803 was shown in Figure 4, which is similar to the biosynthesis of menoquinone in E. coli (Sharma et al., 1996). It is proposed that menF/entC, menD, menE, and menB are responsible for 1,4-dihydroxy-2-naphthoate synthesis. The menA catalyzes the addition of phytyl chain. The gerC2 gene codes for the 2-thytyl-1,4-naphthoquinone methyl transferase enzyme, which catalyzed the methylation step to produce phylloquinone.

To generate a recombinant DNA construction for inactivation of the *menA* gene, two DNA fragment were amplified from *Synechocystis* sp. PCC 6803 genomic DNA by polymerase chain reaction (PCR) (Figure 5). The PstI and ApaI restriction sites were incorporated in both fragments. The first amplification product was digested with EegI and PstI, and the second fragment was digested with PstI and ApaI restriction enzymes. The fragments was ligated with the pBluescript vector, and the kanamycin resistance gene was cloned. The 442-bp part

of the *menA* gene was yielded. The transformation of the wild type strain of *Synechocystis* 6803 and isolation of segregated mutants was performed to obtain the *menA* null strain. The recombinant DNA construct of inactivation of the *menB* gene was generated in the similar way. Two 1.0 kb fragments from upstream and downstream of the *menB* gene were amplified by PCR. The amplified fragments were cloned into pBluescript and a 2.0-kb EcoRI fragment containing the streptomycine/spectinomycine resistance cassettes.
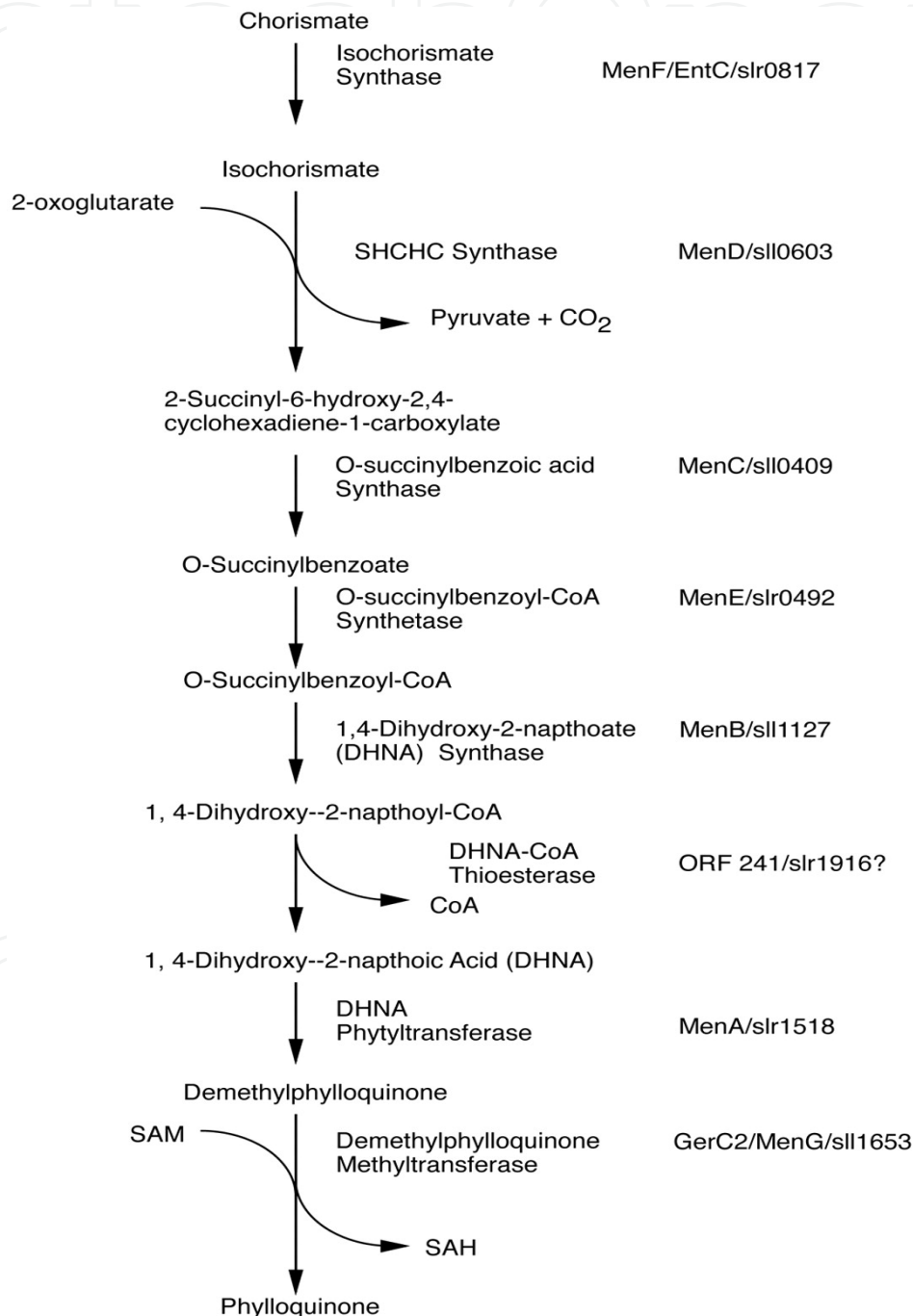

Figure 4. Biosynthetic pathway of phylloquinone in cyanobacterium *Synechocystis* sp. PCC 6803 (Johnson et al., 2000) (Reproduced with permission from the American Society for Biochemistry and Molecular Biology).

In the left of the panel A in Figure 5 shows the restriction maps of the genomic regions surrounding *menA* gene in the wild type and mutant strains. A 440-bp fragment in the *menA* gene was deleted and replaced by a 1.3 kb kanamycine resistance cartridge. PCR amplification of the *menA* locus of the wild type produced the expected 1.9 kb fragment (panel A right, Figure 5). Southern blot hybridization analyses confirmed the interruption of the *menA* gene as expected. Insertional inactivation of the menB gene was also confirmed by both Southern blot hybridization and PCR amplification of menB locus from the mutant strain. The part of the menB gene was deleted and replaced with a 2-kb spectinomycin resistance cartridge (left, panel B in Figure 5). The PCR amplification of the menB locus of the wild type produced the expected fragment of 920 bp (right, panel B in Figure 5), confirming the inactivation of the menB gene.
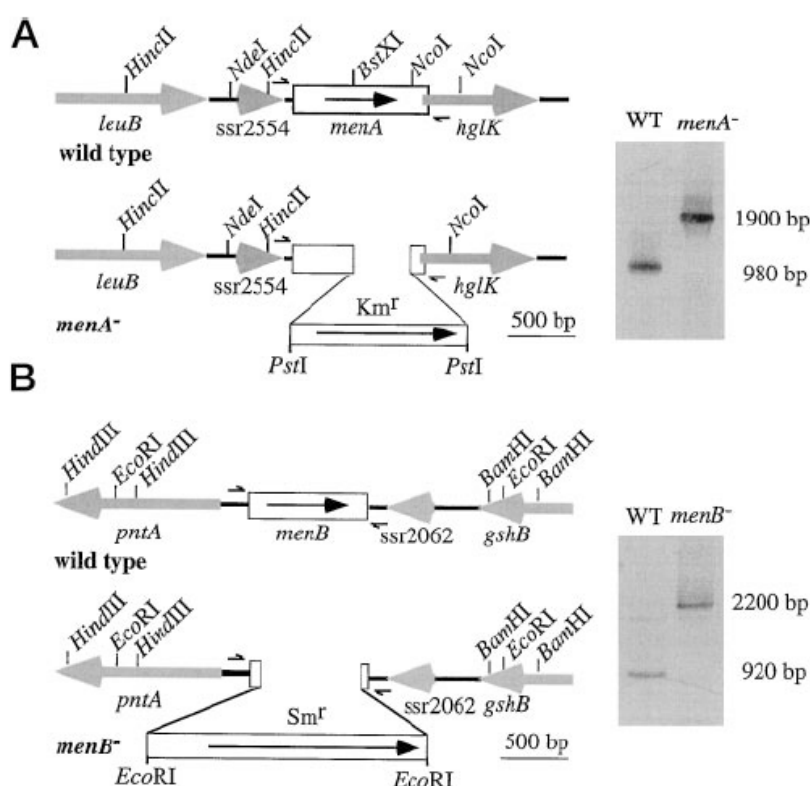

Figure 5. Construct and confirmation of *menA* and *menB* null mutants by inactivation of *menA* and *menB* genes in *Synechocystis* sp. PCC 6803 (Johnson et al., 2000) (Reproduced with permission from the American Society for Biochemistry and Molecular Biology).

3. Physiological, structural, and kinetics of *menA* and *menB* null mutants

The *menA* and *menB* null mutants are able to grow photoheterotrophically and photoautotrophically under low light conditions. The expression level of active PS I in the *menA* and *menB* mutant are 50-60% of the wild type stain. HPLC analysis indicates that the absence of phylloquinone in PS I and that the presence of high level of plastoquinone in PS I (Johnson et al., 2000). EPR, electron nuclear double resonance, and electron spin echo modulation data suggested that the orientation and distance of the foreign quinone A$_P$ are

almost identical to those of the phylloquinone A_1 in the wild type PS I. In addition, EPR measurements show that plastoquinone has been recruited into the A_1 site and functions as an efficient one electron carrier (Zybailov et al., 2000).

As shown in Figure 6, the rates of electron transfer from P_{700} to A_0 and A_1 in the mutants are similar to the wild type PS I. However, the kinetic parameter from A_1 anion to F_x is quite different in the *menA* and *menB* null mutants. The time-resolved optical studies revealed that the forward electron transfer from A_1 anion to F_x is slowed 1000-fold, to 15 and 300 ⊚s, compared to 20 and 200 ns in the wild type PS I (Semenov et al., 2000; Johnson et al., 2001). Based the kinetic data of electron transfer in *menA* and *menB* mutant, the redox potential of A_P in *menA* and *menB* PS I is estimated to be more oxidizing than phylloquinone so that electron transfer from A_P anion to F_x is thermodynamically unfavorable in the mutants (right panel of Figure 6).
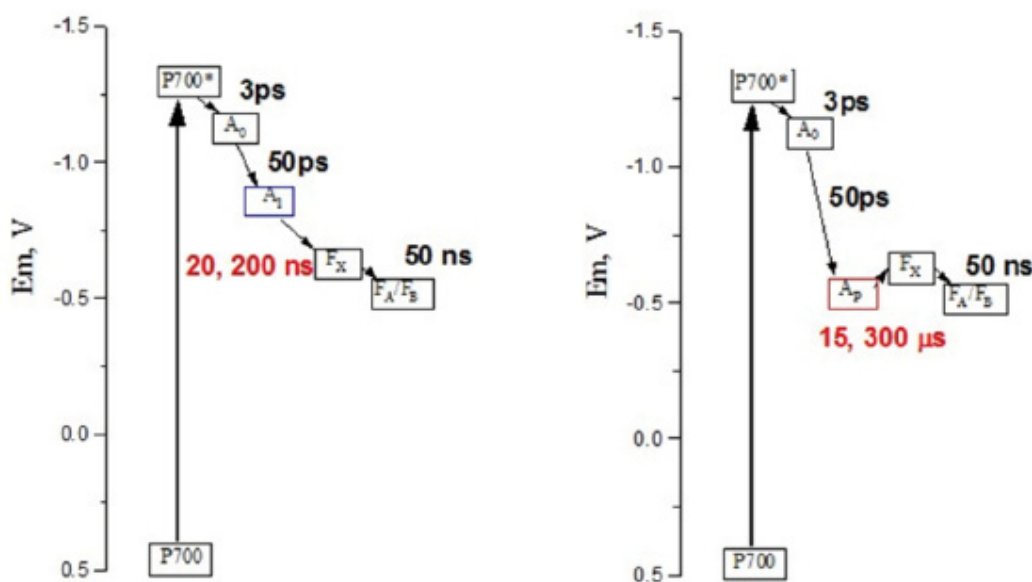

Figure 6. Kinetic data of electron transfer steps in native and *menA/menB* null mutants of *Synechocystis* sp. PCC 6803

4. Thermodynamics of *menA* and *menB* Null Mutants

Pulsed photoacoustic spectroscopy can provide a direct measurement of thermodynamic parameters such as volume change and enthalpy changes that accompany electron transfer reactions (Braslavsky, 1985; Carpentier et al., 1990; Arnaut et al., 1992; Small et al., 1992; Losi et al., 1995; Edens et al., 2000; Malkin, 2000; Herbert et al., 2001; Feitelson and Mauzerall, 2002; Delosme, 2003; Hou and Mauzerall, 2006; Hou and Sakmar, 2010; Hou, 2011; Hou and Mauzerall, 2011). With prior knowledge of the change in Gibbs free energy of the corresponding reactions, the apparent entropy change (TΔS) of the reaction can be calculated. This is an important parameter, knowledge of which is required to fully understand the mechanism of electron transfer, and it has been largely underreported in the literature. The ΔH, ΔV, and TΔS of electron transfer in the photosynthetic reaction center

from *Rb. sphaeroides* have been measured using pulsed photoacoustics (Edens et al., 2000; Nagy et al., 2001). In oxygenic photosynthetic systems, the same parameters of electron transfer in PS I trimers and in Mn depleted PS II reaction center cores from *Synechocystis* sp. PCC 6803 and higher plants have been investigated using similar techniques (Delosme et al., 1994; Hou et al., 2001). These data were confirmed by photoacoustic measurements on whole cells of *Synechocystis* sp. PCC 6803 (Boichenko et al., 2001). The thermodynamic parameters of bacterial reaction centers were found to be similar to those of PS I and dramatically different from those of PS II.

Using the fit by convolution of photoacoustic waves on the nanosecond and microsecond time scales, the thermodynamic parameters of different kinetic steps in *Synechocystis* PS I were resolved (Hou and Mauzerall, 2006). A large negative enthalpy (-0.8 eV) and large volume change (-23 Å^3) for the P_{700}^* to $A_1^-F_X$ step and a positive enthalpy (+0.4 eV) and a small volume change (-3 Å^3) for the $A_1^-F_X$ to $F_{A/B}$-step were observed. For the fast reaction the free energy change for the P_{700}^* $A_1^-F_X$ step is -0.63 eV, and the entropy change (T$\triangle$S, T=25 $^\circ$C) is -0.2 eV. For the slow reaction, $A_1^-F_X$ to $F_{A/B}^-$, the free energy is -0.14 eV (43), and the entropy change (T$\triangle$S) is positive, +0.54 eV. The positive entropy contribution is even larger than the positive enthalpy, indicating that the $A_1^-F_X$ to $F_{A/B}^-$ step in *Synechocystis* PS I is entropy driven.

The photoacoustic waves produced by forming a charge-separated radical pair upon light excitation of PS I trimers consist of at least two major components: (1) the heat output (Q_{RC}), which includes the enthalpy change of the reaction and other rapidly released heat, and (2) the volume change of the reaction (ΔV_{RC}). The thermal signal disappears at the temperature of maximum density of the suspending medium, Tm, near or below 4 $^\circ$C, thus leaving only the volume term (Hou, 2011). Wild-type PS I trimers produced large negative PA signals at 3.8 °C (Figure 7, curve 2) which originate directly from the volume contraction via electrostriction. The volume change in wild-type PS I is -25 Å^3. In contrast, *menA/B* PS I shows a smaller signal (Figure 7, curves 3 and 4). There is no major difference in the volume contraction between *menA* PS I and *menB* PS I. This may be expected since plastoquinone-9 is present in the A_1 sites in PS I in both mutants.

To confirm the values of the volume change and to estimate the quantum yield of charge separation in *menA/B* PS I, two different approaches are utilized: (1) volume yield measurements and (2) saturation measurements. The detailed description of these two procedures has been given previously (Hou et al., 2001; Hou, 2011). The fits of the volume yield curves for the mutants and wild-type PS I are shown in Figure 8. The apparent volume contractions of *menA* PS I and *menB* PS I are -14 and -16 Å^3, respectively, compared to -25 Å^3 for wild-type PS I. In the second saturation method, every PS I complex is excited to obtain the maximum PA signal. In this method, one must calculate the number of PS I centers in the illuminated volume of the cell (~0.34 mL), N, to obtain the real volume change $\triangle$Vs. In this analytical method, the volume change does not contain the quantum yield. As shown in Figure 8, the saturation value of volume change ($\triangle$Vs) in *menA/B* PS I was ~-17 Å^3, which is slightly higher than that using the volume yield method. These findings confirm the previous results and argue that the quantum yield of photochemistry in the mutants is not low.
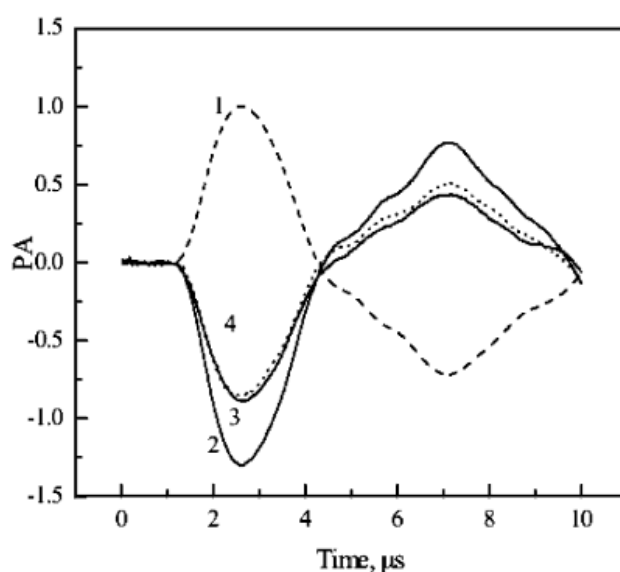
Figure 7. Photoacoustic waves of photosystem I complexes from the photoacoustic reference sample (curve 1), *menA* (curve 3), *menB* (curve 4), and wild-type (curve 2) strains of *Synechocystis* sp. PCC 6803 on the 1-microsecond time scale (Hou et al., 2009) (Reproduced with permission from the American Chemical Society).

The quantum yield of photochemistry can be estimated from measurements of the effective cross section ($\Phi \sigma$). In Figure 8 (lower panel), the quantum yield of charge separation in *menA/B* PS I was estimated to be 85%, a value slightly lower than the 96% quantum yield in wild-type PS I. Taken together, they suggest that the volume contractions in *menA/B* PS I on the microsecond time scale are -17±2 Å^3, and the quantum yields of photochemistry are ca. 85±10%. The observed reaction on the microsecond time scale is attributed to the formation of $P_{700}^+F_{A/B}^-$ from excited P_{700}^* for the wild-type PS I and of $P_{700}^+A_P^-$ for *menA/B* PS I. The enthalpy changes in *menA* and *menB* null mutants were determined to be 0.64±0.1 eV and 0.74±0.1 eV from the difference in slopes in Figure 9, respectively, according to the method described previously (Hou et al., 2001; Hou et al., 2009).

Figure 10 is the typical photoacoustic wave on the fast nanosecond time scale reaction. Curve 1 is the positive signal from a photoacoustic reference at 25 °C, and curves 2, 3, and 4 show large negative signals from wild-type PS I, *menA* PS I, and *menB* PS I, respectively, at 3.8 °C. They indicate that the volume contractions of the mutants are roughly two thirds of the wild type and are similar to those on the microsecond time scale. Figure 11 shows the analysis of photoacoustic data of the mutants and the wild type on the nanosecond time scale. The volume changes during charge separation in *menA/B* PS I were smaller, -17 Å^3, than that of wild type PS I, -21 Å^3. These values are identical to those of the mutants on the microsecond time scale, which indicate that there are no kinetic volume components between the 20 ns and 1 μs time scales in the mutants. It also demonstrates that the photoacoustic methodology on both time scales is reliable. The data in Figure 11 indicate that the enthalpy changes in both mutants are similar, -0.7 eV, which is very close to that on the microsecond time scale.
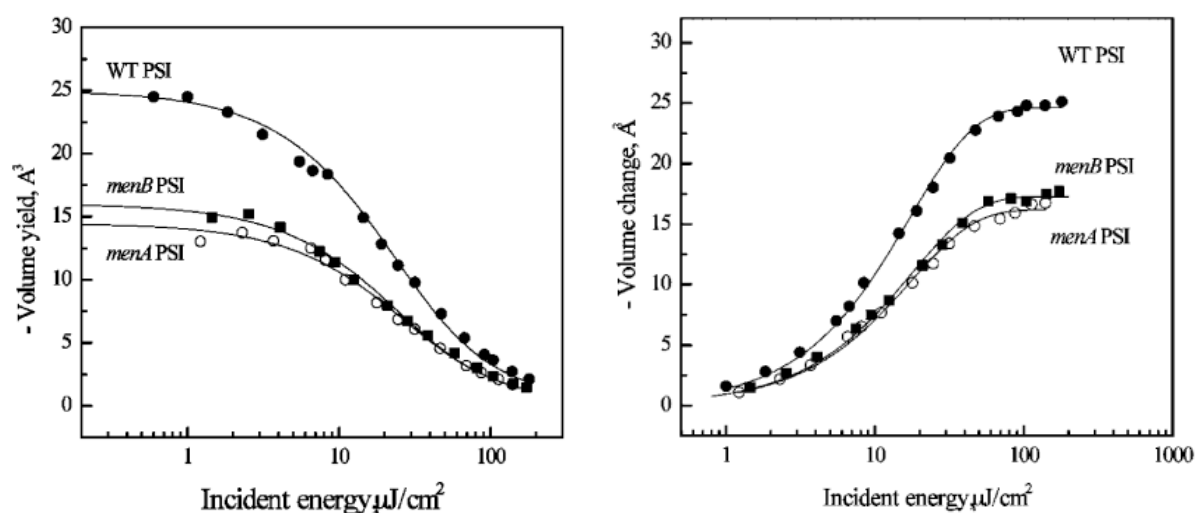
Figure 8. Molecular volume changes determined by volume yield method (left panel) and saturation curve method (right panel) on the 1-microsecond time scale (Hou et al., 2009) (Reproduced with permission from the American Chemical Society).
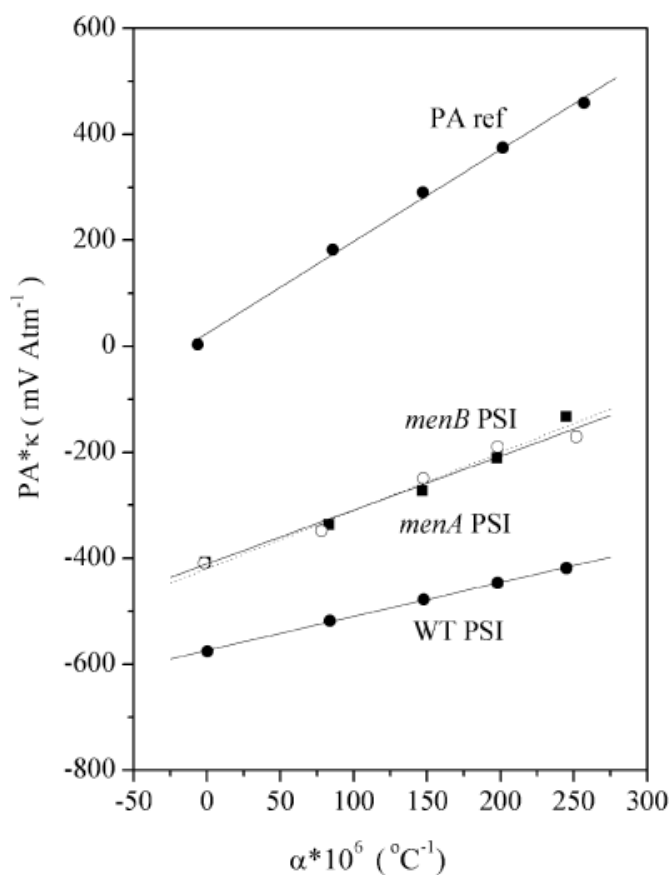

Figure 9. Enthalpy changes determined by analyzing the linear fit of the photoacoustic intensity vs. temperature (water expansitivity) on the 1-microsecond time scale (Hou et al., 2009) (Reproduced with permission from the American Chemical Society).
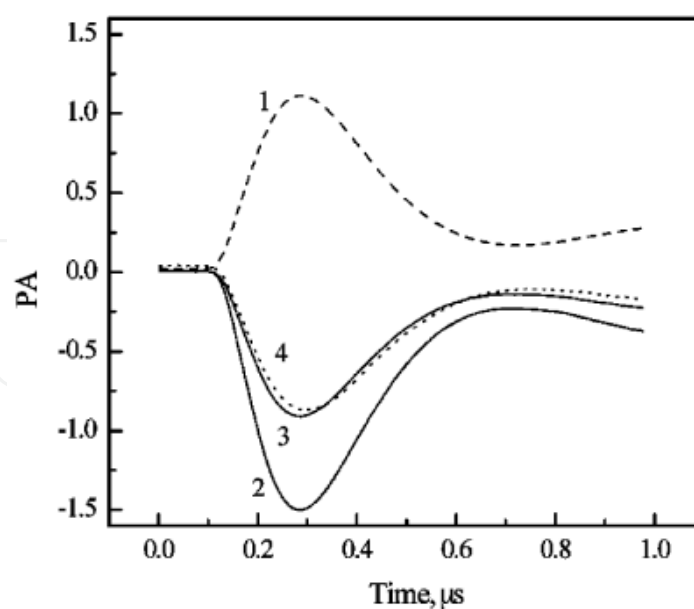
Figure 10. Photoacoustic waves of the photoacoustic reference sample (curve 1), wild-type (curve 2), *menA* (curve 3), and *menB* (curve 4) mutants of *Synechocystis* sp. PCC 6803 on the nanosecond time scale (Hou et al., 2009) (Reproduced with permission from the American Chemical Society).
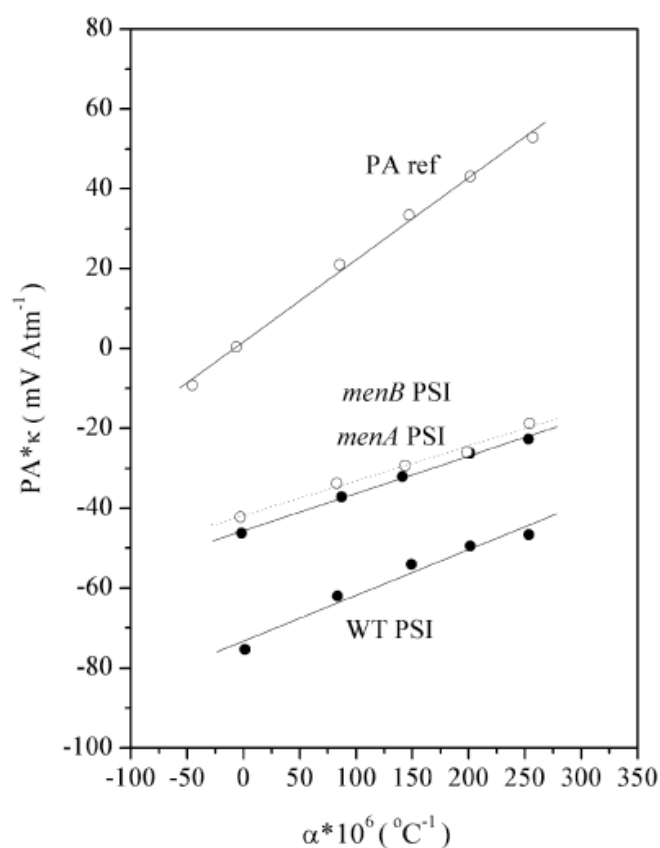

Figure 11. Enthalpy changes determined by plotting the linear fit of the photoacoustic intensity vs. temperature (water expansitivity) on the nanosecond time scale (Hou et al., 2009) (Reproduced with permission from the American Chemical Society).

To summarize the thermodynamic data, the volume changes, free energies, and enthalpy and entropy changes on *menA/B* PS I in comparison with those on the wild-type PS I are listed in Figure 12. Opened arrows are the early step forming $P_{700}^+A_1^-$ from P_{700}^* for the wild-type PS I or $P7_{00}^+A_P^-$ from P_{700}^* for the mutants, and solid arrows are the number of the following reaction: $P_{700}^+A_P^-$ to $P_{700}^+F_{A/B}^-$. As shown in panel A, the volume contraction of the early step of the photoreaction in the mutants (-17 Å^3) is smaller than that in the wild type (-21 Å^3). Similarly, the enthalpy change (-0.7 eV) of the early step in the mutants is smaller than that (-0.8 eV) in wild-type PS I (Figure 12B). Assuming a redox potential of -0.6 V for plastoquinone-9 in the A_1 site (21), the free energy (-0.7 eV) of this early reaction in the mutants is larger than the value (-0.6 eV) in the wild type as indicated in Figure 12C. Taking the difference of free energy and enthalpy change in the mutants, the apparent entropy change of the early step in mutants is zero. In contrast, the apparent entropy change in the wild type is calculated to be +0.2 eV. Since the apparent entropy change for the overall reaction of the generation of $P_{700}^+F_{A/B}^-$ from P_{700}^* is +0.35 eV (32), it implies that the latter reaction in the mutants, i.e., the $P_{700}^+A_P^-F_{A/B}$ to $P_{700}^+A_PF_{A/B}^-$ reaction, is almost completely entropy driven (T$\triangle$S) +0.4 eV and $\triangle$G) -0.1 eV) (Figure 12D).
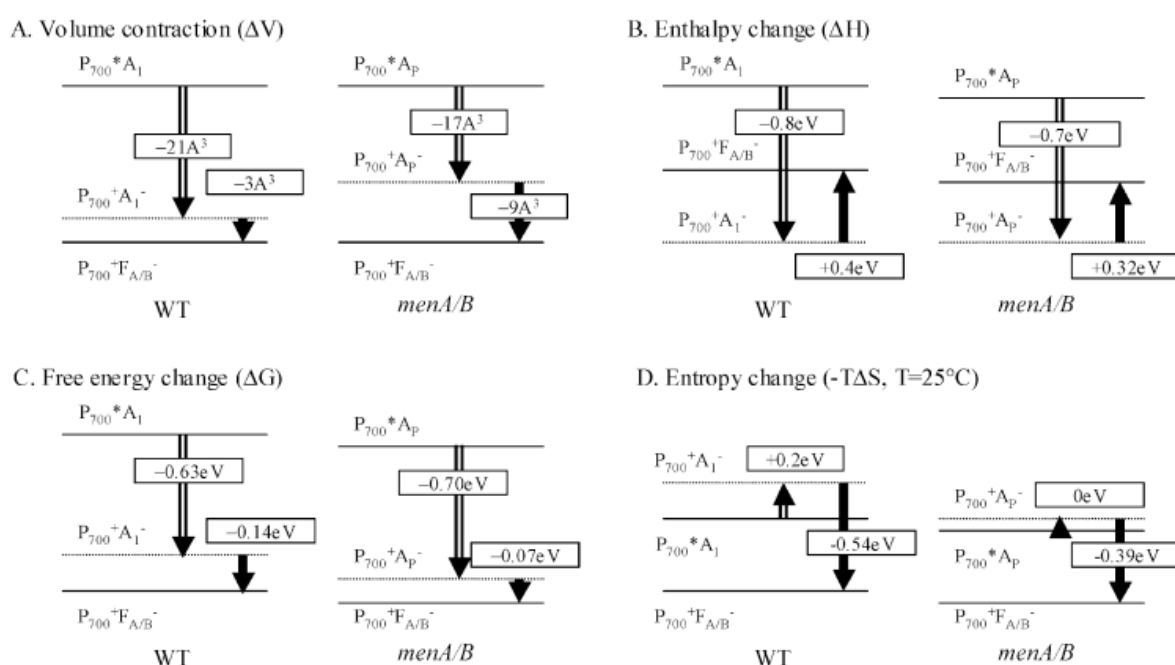

Figure 12. Thermodynamics of electron transfer reactions in photosystem I from the *menA/menB* null mutants and wild-type strains of *Synechocystis* sp. PCC 6803 (Hou et al., 2009) (Reproduced with permission from the American Chemical Society).

In the case of *menA/B* PS I, photoacoustic measurements on the microsecond time scale reveal the volume contraction to be -17 Å^3. Considering our time window of 0.1-10 μ s, this value is assigned to the formation of $P_{700}^+A_P^-$ from $P_{700}^*A_P$. The intermediate step of electron transfer from $P_{700}^+A_P^-F_{A/B}$ to $P_{700}^+A_PF_{A/B}^-$ would be accompanied by a volume change of -9 Å^3, assuming the replacement of A_1 with A_P causes no change in the $F_{A/B}$ clusters. For *menA/B* PS I, the size of the benzoquinone ring in plastoquinone-9 (A_P) is smaller than the

naphthoquinone ring in phylloquinone. Electron spin-echo modulation experiments showed that the distance between P_{700}^+ and A_P^- (25.3 Å) in *menA/B* PS I is the same as the distance between P_{700}^+ and A_1^- in wild-type PS I. The volume contraction of electron transfer from P_{700} to A_P is estimated to be larger (-30 Å^3) than the observed one (-17 Å^3). Thus a positive volume due to a protein conformational change may be possible. We offer a molecular explanation of the difference in the volume change predicted via electrostriction and that of the observed value (-17 Å^3). A simple explanation would be that the quantum yield of photochemistry is lower (for example, ~0.7) in *menA/B* PS I. This, however, is unlikely because our pulse saturation data revealed a quantum yield of ~85% in PS I from both mutants, which is only sufficiently lower than the quantum yield of 96% in wild type PS I to explain less than half of the effect. Further support for a high quantum yield is that the light saturation dependence of the flavodoxin reduction rate in *menA/B* PS I is similar to that of wild-type PS I. These two arguments are consistent in showing that the smaller volume change in the *menA*/B PS I is not caused by a low quantum yield.

The smaller volume contraction may be caused by the following two factors: compressibility of protein and polarity of quinone pocket. The first factor is the effect of the foreign plastoquinone on the compressibility of the local environment of the protein. The orientation and distance of plastoquinone- 9 in the mutants are known to be similar to phylloquinone in the wild-type PS I. However, since the pocket of A_1 is adapted to phylloquinone, the smaller plastoquinone with the longer tail may not fit well into the protein. If the effect of the larger tail is to crowd the hydrophobic site, this could decrease the compressibility of the local domain and so decrease $\triangle V_{el}$. Alternatively, the A_1 binding region in *menA/B* PS I may be more polar; i.e., it has a larger effective ε, compared to the wild-type PS I. This could be due to the small size of plastoquinone-9, allowing a water molecule to be present. This possibility also could explain the change in potential of the quinone because of hydrogen bonding to the water.

By use of the electron transfer theory and kinetic data, the redox potential of plastoquinone at the A_1 site was estimated to be -0.61 V (Hou et al., 2009). However, the error to be at least 0.1 V. The $\triangle G$ for producing $P_{700}^+A_P^-$ from P_{700}^* is then -0.71 eV. Similarly, the free energy for producing $P_{700}^+F_{A/B}^-$ from $P_{700}^*F_{A/B}$ is -0.77 eV (35). Thus we infer that the free energy of $P_{700}^+A_P^-F_{A/B}$ to $P_{700}^+A_PF_{A/B}^-$ reaction is -0.06±0.10 eV in the mutants. Knowing the free energy of the electron transfer step in wild-type PS I and *menA/B* PS I, the entropic contribution (T$\triangle S$) can be determined by the Gibbs relation $\triangle G = \triangle H - T\triangle S$. The enthalpy change occurring on the formation of $P_{700}^+A_P^-$ from P_{700}^* in *menA/B* PS I is -0.7 ± 0.07 eV. This is close to the estimated free energy of this reaction (-0.70 eV), and thus the apparent entropy change is close to zero (Figure 12). Considering the enthalpy change (-0.4 eV) of the overall reaction for the formation of $P_{700}^+F_{A/B}^-$ from P_{700}^* in the wild-type PS I, the electron transfer reaction from A_P^- to $F_{A/B}$ would be associated with a positive enthalpy change of +0.3 eV and thus is completely entropy driven as the free energy is zero in the mutants.

The entropy of electron transfer reactions is often assumed to be zero. However, the free energy calculated from kinetic measurements of reverse electron transfer in bacterial

reaction centers shows that the free energy is time- and temperature dependent, particularly on the less than nanosecond time scale. The kinetics of these decays can only be described as "distributed", and simple analysis in terms of a single component is not trustworthy. Protein dynamics may play a key role in this electron transfer step. However, the question of whether these "relaxations" are enthalpy and/or entropy driven remains to be answered. The slow (microsecond) component observed in wild-type PS I could be such a relaxation, but only the ΔV was determined. The difference between observed enthalpies and estimated free energies as entropies highlights the problem. In addition to reaction centers of Rb. sphaeroides, similar positive entropic contribution in PS I preparations of *Synechocystis* sp. PCC 6803 were observed, but not in PS II preparations. Charge movement, but not charge separation due to proton transfer, may be the difference in PS II on the 1 μs time scale. Clear-cut and large negative entropic contribution is seen in the model system of triplet porphyrin-to-ferricyanide electron transfer in aqueous solution, where "relaxations" are too fast to be relevant.

5. Conclusion

In this chapter, thermodynamics of electron transfers in biological system can be assessed by using a combination of molecular genetics and sophisticated biophysical techniques, in particular, pulsed photoacoustic spectroscopy. Photosynthesis involves light-induced charge separation and subsequently a series of electron transfer reactions and is an ideal system for the detailed study on electron transfer mechanisms in chemistry and biology. In contrast to the susceptible and vulnerable of photosystem II complex to environment, photosystem I complex is much more stable and a perfect choice for such a study. As quinones play a central role in electron transfer reactions in both anoxygenic and oxygenic photosynthesis, the phylloquinone (A_1) of photosystem I is chosen as a probe to explore the effect and regulation of electron cofactors on kinetics and thermodynamics in vivo. The usual approach of chemical modification or replacement of phylloquinone may alter the bonding pocket of the cofactor and the interaction with its proteins.

Molecular genetic technique is utilized to block the biosynthesis of the cofactor, phylloquinone, in the cynobacterium *Synechocystis* sp. PCC 6803 and replace the phylloquinone in the A_1 site with different foreign quinones. The effect of the foreign quinones on the electron transfer is systematically studied by biophysical methodologies. Specifically, the *menA* and *menB* genes, which code for phytyl transferase and 1.4-dihydroxy-2-naphthoae synthase, respectively, are inactivated to prevent the synthesis of phylloquinone. In spite of the demonstrated absence of phylloquinone, the *menA* and *menB* null mutants grow photoheterotrophically. HPLC and EPR measurement show that plastoquinone-9 (A_P) has been recruited into the A_1 site and functions as an efficient one-electron transfer carrier. The orientation and distance between the plastoquinone and other cofactors are the same as that of the wild type. Time-resolved optical studies indicate that the forward electron transfer from A_1 anion to the iron-sulfur cluster (F_X) is slowed 1000-

fold, to 15 to 300 μs, compared to 20 and 200 ns in the wild type. Using the electron transfer theory and kinetic data, the redox potential of plastoquinone at the A_1 site was estimated to be -0.61 V, more oxidizing that phylloquinone. The electron transfer from A_P anion to F_X is thermodynamically unfavorable in the *menA* and *menB* null mutants.

Photoacoustic measurements reveal that the quantum yield of charge separation in *menA* and *menB* is slightly lower (85%) than that of the wild type. The thermodynamic parameters of the two electron transfer steps, including molecular volume changes, reaction enthalpy and apparent entropy, were obtained in *menA* and *menB* null mutants and are considerable different from the wild type. The experimental data demonstrates that the not only the kinetics but also the thermodynamics of electron transfer reaction in photosystem I are affected by the recruitment of the foreign quinone into the A_1 site. One of the most intriguing conclusions is that although free energy for the electron transfer from A_P anion to F_X in *menA* and *menB* mutant is close to zero, the apparent entropy ($T\triangle S$) for this reaction is positive, +0.4 eV. This indicates that the entropy plays a key role in the electron transfer from A_P anion to F_X. As shown in Figure 13, the electron transfer from P_{700} to A_1 is enthalpy driven; the electron transfer from A_1 to F_A/F_B is entropy driven. The driving force of electron transfer in photosynthetic systems is not only dependent on the bonding energy of the cofactor and interaction energy with the protein (enthalpy) but also dependent on the available states of interaction with the protein (entropy).
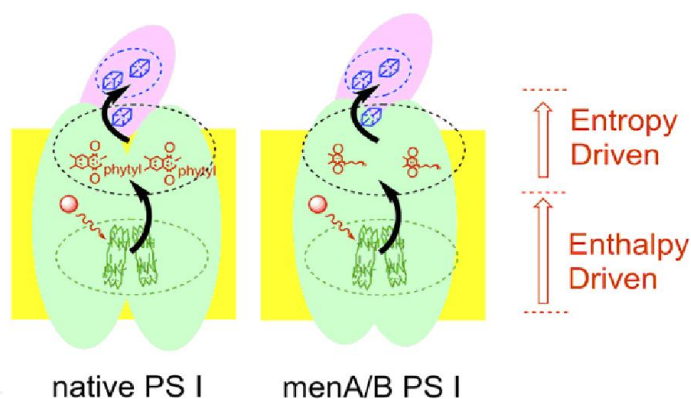

Figure 13. The enthalpy and entropy driven steps in *Synechocystis* 6803 photosystem I

Author details

Xuejing Hou
University of Massachusetts Dartmouth, USA

Harvey J.M. Hou[*]
University of Massachusetts Dartmouth, USA
Alabama State University, USA

[*] Corresponding Author

Acknowledgement

6. References

Arnaut LG, Caldwell RA, Elbert JE, Melton LA (1992) Recent advances in photoacoustic calorimetry: theoretical basis and improvements in experimental design. Rev. Sci. Instrum. 63: 5381-5389

Blankenship RE (2002) Molecular Mechanisms of Photosynthesis. Blackwell Science

Boichenko VA, Hou J-M, Mauzerall D (2001) Thermodynamics of Electron Transfer in Oxygenic Photosynthetic Reaction Centers: Volume Change, Enthalpy, and Entropy of Electron-Transfer Reactions in the Intact Cells of the Cyanobacterium *Synechocystis* PCC 6803. Biochemistry 40: 7126-7132

Braslavsky SE (1985) Time-resolved photoacoustic and photothermal methods. Application to substances of biological interest. NATO ASI Series, Series A: Life Sciences 85: 147-158

Carpentier R, Leblanc RM, Mimeault M (1990) On the nature of the photosynthetic energy storage monitored by photoacoustic spectroscopy. Photosynth. Res. 23: 313-318

Cook TR, Dogutan DK, Reece SY, Surendranath Y, Teets TS, Nocera Daniel G (2010) Solar energy supply and storage for the legacy and nonlegacy worlds. Chem. Rev. 110: 6474-6502

Delosme R (2003) On some aspects of photosynthesis revealed by photoacoustic studies: a critical evaluation. Photosynth. Res. 76: 289-301

Delosme R, Beal D, Joliot P (1994) Photoacoustic detection of flash-induced charge separation in photosynthetic systems. Spectral dependence of the quantum yield. Biochim. Biophys. Acta, 1185: 56-64

Diner BA, Rappaport F (2002) Structure, dynamics, and energetics of the primary photochemistry of photosystem II of oxygenic photosynthesis. Annu. Rev. Plant Biol. 53: 551-580

Edens GJ, Gunner MR, Xu Q, Mauzerall D (2000) The Enthalpy and Entropy of Reaction for Formation of $P^+Q_A^-$ from Excited Reaction Centers of *Rhodobacter sphaeroides*. J. Am. Chem. Soc.122: 1479-1485

Feitelson J, Mauzerall D (2002) Enthalpy and Electrostriction in the Electron-Transfer Reaction between Triplet Zinc Uroporphyrin and Ferricyanide. J. Phys. Chem. B 106: 9674-9678

Golbeck JH, (2006) Photosystem I; The Light-Driven Plastocyanin: Ferredoxin Oxidoreductase. Springer

Gunner MR, Dutton PL (1989) Temperature and $\Delta G°$ dependence of the electron transfer from BPh⁻ to Q_A in reaction center protein from *Rhodobacter sphaeroides* with different quinones as Q_A. J. Am. Chem. Soc. 111: 3400-3412

Herbert SK, Han T, Vogelmann TC (2001) New applications of photoacoustics to the study of photosynthesis. Photosynth. Res. 66: 13-31

Hou HJM (2010) Structural and mechanistic aspects of Mn-oxo and Co-based compounds in water oxidation catalysis and potential application in solar fuel production. J. Integr. Plant Biol. 52: 704-711

Hou HJM (2011) Enthalpy, entropy, and voluem changes of electron transfer reactions in photosynthetic proteins, In: Application of thermodynamics to biological and material science, Mizutani Tadashi Ed., Intech, pp. 93-110.

Hou HJM (2011) Manganese-based materials inspired by photosynthesis for water-splitting. Materials 4: 1693-1704

Hou HJM, Mauzerall D (2006) The $A_1^-F_X$ to $F_{A/B}$ Step in *Synechocystis* 6803 Photosystem I Is Entropy Driven. J. Am. Chem. Soc. 128: 1580-1586

Hou HJM, Mauzerall D (2011) Listening to PS II: Enthalpy, entrhopy and volume changes. J. Photochem. Photobiol. B 104: 357-365

Hou HJM, Sakmar TP (2010) Methodology of pulsed photoacoustics and its application to probe photosystems and receptors. Sensors 10: 5642-5667

Hou HJM, Shen G, Boichenko VA, Golbeck JH, Mauzerall D (2009) Thermodynamics of Charge Separation of Photosystem I in the *menA* and *menB* Null Mutants of *Synechocystis* sp. PCC 6803 Determined by Pulsed Photoacoustics. Biochemistry 48: 1829-1837

Hou JM, Boichenko VA, Wang YC, Chitnis PR, Mauzerall D (2001) Thermodynamics of electron transfer in oxygenic photosynthetic reaction centers: a pulsed photoacoustic study of electron transfer in photosystem I reveals a similarity to bacterial reaction centers in both volume change and entropy. Biochemistry 40: 7109-7116

Johnson TW, Shen G, Zybailov B, Kolling D, Reategui R, Beauparlant S, Vassiliev IR, Bryant DA, Jones AD, Golbeck JH, Chitnis PR (2000) Recruitment of a foreign quinone into the A_1 site of photosystem I. I. Genetic and physiological characterization of phylloquinone biosynthetic pathway mutants in *Synechocystis* sp. pcc 6803. J. Biol. Chem. 275: 8523-8530

Johnson TW, Zybailov B, Jones AD, Bittl R, Zech S, Stehlik D, Golbeck JH, Chitnis PR (2001) Recruitment of a foreign quinone into the A_1 site of photosystem I. In vivo replacement of plastoquinone-9 by media-supplemented naphthoquinones in phylloquinone biosynthetic pathway mutants of *Synechocystis* sp. PCC 6803. J. Biol. Chem. 276: 39512-39521

Jordan P, Fromme P, Witt HT, Klukas O, Saenger W, Krauss N (2001) Three-dimensional structure of cyanobacterial photosystem I at 2.5 A resolution. Nature 411: 909-917

Kamlowski A, Altenberg-Greulich B, Van der Est A, Zech SG, Bittl R, Fromme P, Lubitz W, Stehlik D (1998) The Quinone Acceptor A_1 in Photosystem I: Binding Site, and Comparison to Q_A in Purple Bacteria Reaction Centers. J. Phys. Chem. B 102: 8278-8287

Kanan M, Nocera DG (2008) In Situ Formation of an Oxygen-Evolving Catalyst in Neutral Water Containing Phosphate and Co^{2+}. Science 321: 1072 - 1075

Lewis NS, Nocera DG (2006) Powering the planet: chemical challenges in solar energy utilization. Proc. Natl. Acad. Sci. U S A 103: 15729-15735

Losi A, Bedotti R, Viappiani C (1995) Time-Resolved Photoacoustics Determination of Intersystem Crossing and Singlet Oxygen Photosensitization Quantum Yields for 4,5',8-Trimethylpsoralen. J. Phys. Chem. 99: 16162-16167

Malkin S (2000) The photoacoustic effect in leaves and its applications. Probing In: Probing Photosynthesis: Mechanism, Regulation & Adaptation, M Yunus, U Pathre, and P Mohanty Eds., Taylor & Francis, pp. 484-524

Mauzerall D (2006) Thermodynamics in photosystem I. In: Photosystem I: The Light-Driven Plastocyanin: Ferredoxin Oxidoreductase, J Golbeck ed., Springer, pp. 571-581

Nagy L, Kiss V, Brumfeld V, Malkin S (2001) Thermal and structural changes of photosynthetic reaction centers characterized by photoacoustic detection with a broad frequency band hydrophone. Photochem. Photobiol. 74: 81-87

Semenov AY, Vassiliev IR, van Der Est A, Mamedov MD, Zybailov B, Shen G, Stehlik D, Diner BA, Chitnis PR, Golbeck JH (2000) Recruitment of a foreign quinone into the A_1 site of photosystem I. Altered kinetics of electron transfer in phylloquinone biosynthetic pathway mutants studied by time-resolved optical, EPR, and electrometric techniques.J. Biol. Chem. 275: 23429-23438

Semenov AY, Vassiliev IR, Van der Est A, Mamedov MD, Zybailov B, Shen G, Stehlik D, Diner BA, Chitnis PR, Golbeck JH (2000) Recruitment of a foreign quinone into the A_1 site of photosystem I. Altered kinetics of electron transfer in phylloquinone biosynthetic pathway mutants studied by time-resolved optical, EPR, and electrometric techniques. J. Biol. Chem. 275: 23429-23438

Sharma V, Hudspeth ME, Meganathan R (1996) Gene 168: 43-48

Small JR, Libertini LJ, Small EW (1992) Analysis of photoacoustic waveforms using the nonlinear least squares method. Biophys. Chem. 42: 29-48

Tadashi M (2011) Application of Thermodynamics to Biological and Materials Science. Intech

Zybailov B, van der Est A, Zech SG, Teutloff C, Johnson TW, Shen G, Bittl R, Stehlik D, Chitnis PR, Golbeck JH (2000) Recruitment of a foreign quinone into the A_1 site of photosystem I. II. Structural and functional characterization of phylloquinone biosynthetic pathway mutants by electron paramagnetic resonance and electron-nuclear double resonance spectroscopy. J. Biol. Chem. 275: 8531-8539